Understanding the role of Si doping on surface charge and optical properties: Photoluminescence study of intrinsic and Si-doped InN nanowires

S. Zhao, Z. Mi,* and M. G. Kibria
Department of Electrical and Computer Engineering, McGill University, 3480 University Street, Montreal, Quebec, Canada H3A 2A7

Q. Li and G. T. Wang
Advanced Materials Sciences, Sandia National Laboratories, Albuquerque, New Mexico 87185, USA
(Received 23 March 2012; published 20 June 2012)

In the present work, the photoluminescence (PL) characteristics of intrinsic and Si-doped InN nanowires are studied in detail. For intrinsic InN nanowires, the emission is due to band-to-band carrier recombination with the peak energy at ∼0.64 eV (at 300 K) and may involve free-exciton emission at low temperatures. The PL spectra exhibit a strong dependence on optical excitation power and temperature, which can be well characterized by the presence of very low residual electron density and the absence or a negligible level of surface electron accumulation. In comparison, the emission of Si-doped InN nanowires is characterized by the presence of two distinct peaks located at ∼0.65 and ∼0.73–0.75 eV (at 300 K). Detailed studies further suggest that these low-energy and high-energy peaks can be ascribed to band-to-band carrier recombination in the relatively low-doped nanowire bulk region and Mahan exciton emission in the high-doped nanowire near-surface region, respectively; this is a natural consequence of dopant surface segregation. The resulting surface electron accumulation and Fermi-level pinning, due to the enhanced surface doping, are confirmed by angle-resolved x-ray photoelectron spectroscopy measurements on Si-doped InN nanowires, which is in direct contrast to the absence or a negligible level of surface electron accumulation in intrinsic InN nanowires. This work elucidates the role of charge-carrier concentration and distribution on the optical properties of InN nanowires.

DOI: 10.1103/PhysRevB.85.245313 PACS number(s): 81.05.Ea, 78.55.Cr

I. INTRODUCTION

InN, after being discovered with a narrow band gap ($E_g \sim 0.65$–1 eV)[1–14] and predicted to possess the largest electron mobility among group-III nitrides (∼4400 $cm^2\ V^{-1}\ s^{-1}$ at 300 K),[15] has emerged as a highly promising material for infrared photodetectors and lasers, solar cells, ultrahigh-speed transistors, and sensors.[16–18] To date, however, the practical device applications of InN-based materials have been severely limited by the presence of extremely large residual electron density and the uncontrolled surface charge properties as well as the difficulty in achieving p-type conductivity.[8,19–30] For example, in general, the currently reported nominally undoped InN is n-type degenerate, with the residual electron densities in the range of $\sim 1\times 10^{18}$ cm^{-3} or higher.[8,11,25,31–34] Moreover, it has been generally observed that there exists a very high electron concentration ($\sim 1 \times 10^{13-14}$ cm^{-2}) at both the polar and nonpolar *grown* surfaces of InN films,[19,35] and the Fermi-level (E_F) is pinned deep into the conduction band at the surfaces;[19,20,29,30] a similar electron accumulation profile has also been measured at the lateral nonpolar *grown* surfaces of [0001]-oriented wurtzite InN nanowires.[8,11,21,22,25,36]

In this regard, significant efforts have been devoted to understanding the fundamental surface charge properties of InN.[20,23,27,29,30,37–39] The electron accumulation at polar InN surface has been explained by the presence of a large density of the occupied In-In bond states above the conduction-band minimum (CBM)[23] as well as the unusual positioning of the branch point energy E_B well above the CBM at the Γ point, which allows donor-type surface states to exist in the conduction band;[20] for polar InN surface, theoretical studies agree well with experiments. In terms of nonpolar InN surface, recent studies suggest that the surface electron accumulation may depend critically on the surface states, impurities, stoichiometry, and polarity,[27,37] and the absence of electron accumulation at nonpolar surface has been predicted.[23,27] In experiments, however, only recent cross-sectional scanning photoelectron microscopy and spectroscopy studies at a nonpolar *cleaved* InN surface exhibit the unpinned E_F,[38,39] while in general the electron accumulation has prevalently been observed at nonpolar InN surface;[22,34,35] the electron accumulation issue at nonpolar InN surface had remained elusive.

On the other hand, the photoluminescence (PL) properties of InN films have been investigated intensively,[6,7,9,40–44] and the PL emission characteristics are strongly dependent on the residual electron concentrations. For a low residual electron concentration, band-to-band recombination is suggested,[6,7,10,41] while for a high residual electron concentration, Mahan excitons,[40] i.e., photons produced via recombination between electrons near E_F and localized photogenerated holes, are believed to be the underlying recombination mechanism.[7,9,40] Meanwhile, significant efforts have also been made to study the optical properties of InN nanowires.[8,11,21,24,28,33,45] The PL spectra of nominally undoped InN nanowires typically exhibit a very large inhomogeneous broadening, a peak energy considerably larger than the band gap of InN, and an anomalous dependence on temperature. Due to these strong n-type characteristics of nominally undoped InN nanowires, the optical properties of intrinsic InN nanowires and the dependence on the charge-carrier concentrations and surface charge properties had remained unclear.

Recently, with the use of an *in situ* deposited In seeding layer, high-quality InN nanowires with extremely low residual electron densities in the range of $\sim 1 \times 10^{15-16}$ cm^{-3} were achieved on Si (111) substrate by radio-frequency

plasma-assisted molecular beam epitaxy (RF-PAMBE).[12,13,46] With such low residual electron densities, studying the fundamental carrier dynamics as well as the correlated electrical and optical properties of InN nanowires with controlled charge-carrier concentration becomes possible.

In the present paper, both undoped and Si-doped InN (InN:Si) nanowires were grown on Si (111) substrate with the aforementioned RF-PAMBE process. Their PL characteristics and surface charge properties were subsequently investigated using the temperature-variable micro-PL spectroscopy and angle-resolved x-ray photoelectron spectroscopy (XPS). It was observed that the PL emission of intrinsic InN nanowires can be ascribed to band-to-band carrier recombination and may involve free-exciton emission at low temperatures.

Compared to the intrinsic InN nanowires, InN:Si nanowires exhibit two distinct emission peaks, which are centered at ~0.65 and ~0.73–0.75 eV (at 300 K), respectively. Detailed power- and temperature-dependent PL analysis suggests that these low-energy and high-energy peaks are directly related to band-to-band carrier recombination and Mahan exciton emission, respectively. This can be well explained by the significantly enhanced Si-dopant incorporation in the near-surface region of InN:Si nanowires, which is further confirmed by the near-surface E_F pining (~0.35 eV above the CBM) measured in such InN:Si nanowires. As a comparison, the near-surface E_F is located well below the CBM for the intrinsic InN nanowires.

This study has elucidated the fundamental carrier recombination processes in intrinsic InN nanowires. In addition, we have further identified the role of charge-carrier concentration, as well as the inhomogeneous charge-carrier distribution due to the predominant influence of enhanced surface doping, on PL characteristics of InN:Si nanowires.

This paper is organized as follows. In Sec. II, the experimental methods, including RF-PAMBE, micro-PL, and XPS measurements, are presented. In Sec. III, the PL emission characteristics for both undoped and Si-doped InN nanowires are described. A detailed discussion of the carrier recombination and PL emission mechanisms as well as the surface charge properties is presented in Sec. IV. Finally, conclusions are made in Sec. V.

II. EXPERIMENTAL SETUPS

Undoped and Si-doped InN nanowires were grown using a catalyst-free process on Si (111) substrate by RF-PAMBE, with a substrate temperature of $T \sim 480$ °C, In flux of $\sim 6 \times 10^{-8}$ Torr, RF plasma forward power of ~350 W, and a nitrogen flow rate of ~1.0 SCCM (SCCM denotes cubic centimeter per minute at STP). For InN:Si nanowires, the Si cell temperatures were ~1250 °C and ~1350 °C, respectively. Compared to the previous approaches in growing InN nanowires,[8,21,32,36,47–51] in this experiment an In seeding layer (~0.6 nm) was first deposited *in situ* onto Si (111) surface prior to the growth initiation, which can promote the formation and nucleation of InN nanowires. The detailed growth procedures are described elsewhere.[12,46]

A high-resolution scanning electron microscopy (HRSEM) image of undoped InN nanowires is shown in Fig. 1, which exhibits near-perfect hexagonal structure. The nanowires are oriented along the [0001] polar direction, with their sidewalls being nonpolar m planes. Detailed transmission electron microscopy (TEM) studies further confirm that such undoped InN nanowires are nearly free of defects and dislocations.[12] It should be noted that this nontapered hexagonal structure can be achieved in InN:Si nanowires as well (HRSEM images not shown here). In this study, experiments (unless otherwise stated) were performed on InN nanowires with lengths of ~0.7–0.8 μm.

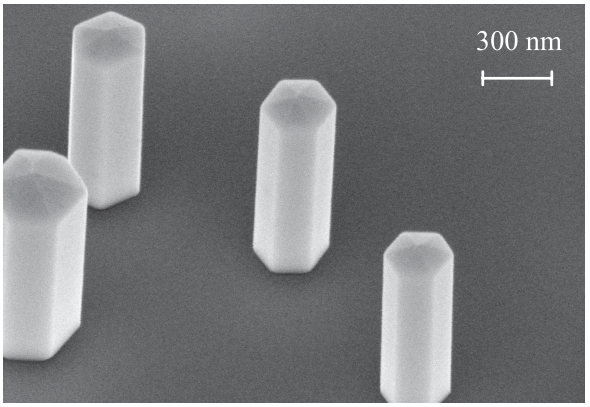

FIG. 1. HRSEM image of undoped InN nanowires taken at a 45° angle. It should be noted that this near-perfect hexagonal wurtzite structure is also maintained in InN:Si nanowires.

Micro-PL measurements were performed on such as-grown InN nanowires at both cryogenic and room temperatures. The nanowires were optically excited using a semiconductor diode laser with $\lambda = 635$ nm through a 100× objective. The defocused beam size is ~5 μm. The emitted light from the nanowires, going through the same 100× objective, was spectrally resolved by a high-resolution spectrometer and detected by a liquid-nitrogen-cooled InGaAs detector with a cutoff wavelength of 2.2 μm. The signal was collected with a single-channel lock-in amplifier.

Angle-resolved XPS was employed as a direct probe of the near-surface E_F in undoped and Si-doped InN nanowires. In this experiment, the x-ray beam was impinged upon the nanowire lateral surfaces, with the resulting photoelectrons being collected at a near-zero takeoff angle. The measurement configuration ensures that the majority of the signal is derived from the nanowire sidewalls.

III. EXPERIMENTAL RESULTS

A. PL spectra of undoped InN nanowires

The PL emission properties of undoped InN nanowires were investigated first. Figure 2(a) shows the temperature-dependent PL spectra measured under an excitation power of 9 mW. It can be seen that, as the temperature increases, the PL peak E^1_{PL} shifts to lower energies and the spectra become broader. The derived temperature dependence of E^1_{PL} is shown in Fig. 2(b). Such a temperature-dependent peak energy can be phenomenally fitted by Varshni's

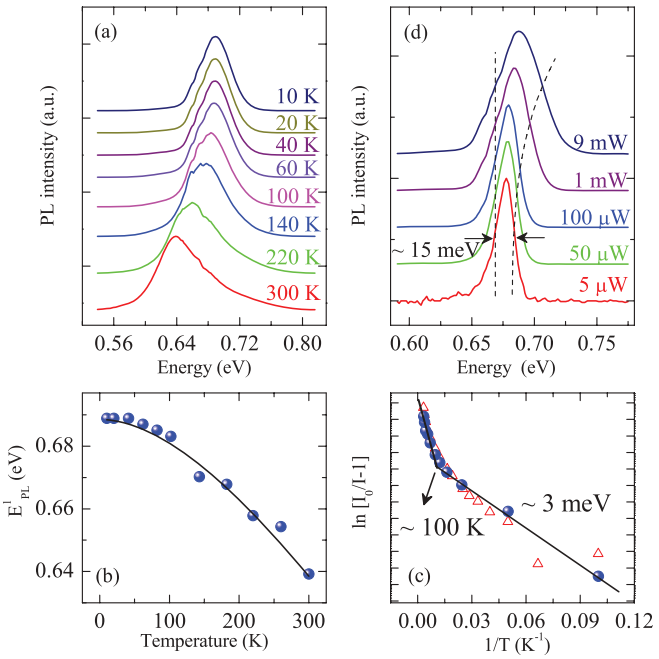

FIG. 2. (Color online) (a) Temperature-dependent PL spectra of undoped InN nanowires measured under an optical excitation power of 9 mW. (b) Temperature dependence of E^1_{PL}; the solid line is the curve fitted using Varshni's equation. (c) Scaling plot of integrated PL intensity I, as described in the text. (d) Power-dependent PL spectra measured at 20 K. The arrows denote the FWHM position, and the dotted vertical line and the dotted curve exhibit the evolution of the FWHM.

equation,

$$E_g(T) = E_g(0) - \frac{\alpha T^2}{\beta + T}, \tag{1}$$

where $E_g(0)$ is the fundamental band gap and α and β are Varshni's coefficients, which correspond to the lattice thermal expansion and the Debye temperature, respectively.[10,18] As shown in Fig. 2(b), the best fit gives $E_g(0) = 0.689 \pm 0.001$ eV, $\alpha = 0.41 \pm 0.02$ meV/K, and $\beta = 449 \pm 32$ K; these values are consistent with those obtained from absorption spectra and PL spectra measurements in InN films,[5,10,18,52] suggesting the nature of this PL emission is band-to-band carrier recombination. This result is in direct contrast to the nearly temperature-invariant PL emission characteristics of n-type degenerate InN nanowires.[8,21,33]

It should be noted that the PL peak energy in general is not equivalent to band-gap energy; it is only approximately valid when under very low excitation conditions and in the absence of localized states and the band-tailing effect.[6] Table I shows the extracted $E_g(0)$, α, and β values measured under different optical excitation conditions with different nanowire lengths. It can be seen that in the lowest photogenerated carrier density regime (with an 0.8-μm nanowire length, 1-mW excitation power, and 50-μm beam size), $E_g(0)$ is ~0.672 eV; this value is consistent with the smallest reported $E_g(0)$ in InN epilayers.[10]

We have further investigated the integrated PL intensity as a function of temperature, which provides more insight

TABLE I. Varshni's parameters extracted from the PL spectra of InN nanowires with different lengths measured under different optical excitation conditions.

Length, power	$E_g(0)$ (eV)	α (meV/K)	β (K)
0.8 μm, 9 mW	0.689	0.41	449
4 μm, 9 mW	0.674	0.44	445
4 μm, 1 mW	0.674	0.44	502
0.8 μm, 1 mW[a]	0.672	0.30	467

[a]With a larger beam size of 50 μm.

of the underlying mechanism(s) of carrier recombination. As illustrated in Fig. 2(c), $\ln[I_0/I - 1]$ is plotted as a function $1/T$ under an excitation power of 9 mW, where I_0 is the maximum PL intensity at low temperature and I represents the integrated PL intensity measured at various temperatures. It can be seen that there exist two distinct slopes, which change at ~100 K (about ~8 meV); this slope-change temperature sets an upper limit of the exciton binding energy,[53–55] which is consistent with the previously reported value of ~9 meV from Wu.[18] Additionally, the exciton binding energy is suggested to be related to the activation energy derived in the low-temperature range (10–100 K),[56,57] which is ~3 meV in this study. This small activation energy is consistent with the derived exciton binding energy of ~2–3 meV if assuming an InN dielectric constant $\epsilon \sim 14$ and an effective mass for electrons $m_e^* = 0.05m_0$ and an effective mass for holes $m_h^* = 0.3m_0$.[6,41,58,59] These studies suggest the recombination process changes from free-exciton emission at low temperatures to electron-hole plasma emission at high temperatures in the presented undoped InN nanowires. Such measurements were also performed on undoped InN nanowires with lengths up to ~4 μm, which show similar scaling behavior [see open triangles in Fig. 2(c)].

Figure 2(d) shows the power-dependent PL spectra of undoped InN nanowires measured at 20 K. At low excitation conditions (<1 mW), variations of the integrated PL intensity I with optical excitation power P can be described by $I \propto P^{0.99\pm0.18}$. This nearly linear I-P dependence further confirms that the emission is directly related to free-exciton recombination at low temperatures.[60] At high excitation conditions (>1 mW), a significant blueshift of E^1_{PL}, accompanied by a spectral linewidth broadening, was observed, which is consistent with the band-filling effect.[13] It may also be noted that, with increasing optical excitation power, the high-energy side of the PL spectra becomes significantly broader (see the dotted curve), which is a direct reflection of the E_F shifting into the conduction band. On the other hand, the low-energy side of the PL spectra does not show any variation with increasing optical excitation power (see the vertical dotted line), suggesting the absence or negligible level of the band-tailing effect and localized states.

The PL peak energy and the linewidth measured at 20 K under 5-μW optical excitation power are ~0.675 eV and ~15 meV, respectively. These values are considerably smaller than commonly reported values for n-type degenerate InN nanowires/nanorods.[8,21,33] Under very low excitation

conditions (not shown here), extremely narrow spectral linewidths, in the range of ∼9–12 meV, have been measured for undoped InN nanowires.[61] A detailed analysis of such undoped InN nanowires shows that the residual electron densities are in the range of $\sim 4 \times 10^{15}$ cm^{-3} or lower,[46] compared to the commonly reported values of $\sim 1 \times 10^{18-19}$ cm^{-3} for n-type degenerate InN nanowires/nanorods.[8,21,25]

B. PL spectra of Si-doped InN nanowires

With the distinct PL characteristics of undoped InN nanowires described above, we can investigate the PL characteristics of InN nanowires with controlled n-type doping. In what follows, we describe the temperature- and power-dependent PL characteristics of InN:Si nanowires with Si cell temperatures of 1250 °C (defined as "moderately Si doped") and 1350 °C (defined as "heavily Si doped"), which correspond to average doping concentrations of approximately 5×10^{17} and 5×10^{18} cm^{-3}, respectively.[62]

The PL characteristics of moderately Si-doped InN nanowires are described first. As illustrated in Fig. 3(a), it can be seen that at low temperatures (<160 K), the PL spectra are characterized by a single emission peak, with peak energy $E^H_{\rm PL} \sim 0.73$ eV. This energy is considerably larger than that of undoped InN nanowires [$E^1_{\rm PL}$, shown in Fig. 2(a)]. Such a large PL peak energy has been commonly measured for n-type degenerate InN nanowires.[8,21,33] When the temperature increases, however, in contrast to n-type degenerate InN nanowires, it is observed that a low-energy peak $E^L_{\rm PL} \sim 0.65$ eV (at 300 K) emerges in the PL spectra. The arrow in Fig. 3(a) shows the trend of $E^L_{\rm PL}$ evolving with the temperature. At 300 K, the intensity of $E^L_{\rm PL}$ is observably higher than that of $E^H_{\rm PL}$, suggesting $E^L_{\rm PL}$ is not likely a phonon replica (second-order effect) of the high-energy peak.

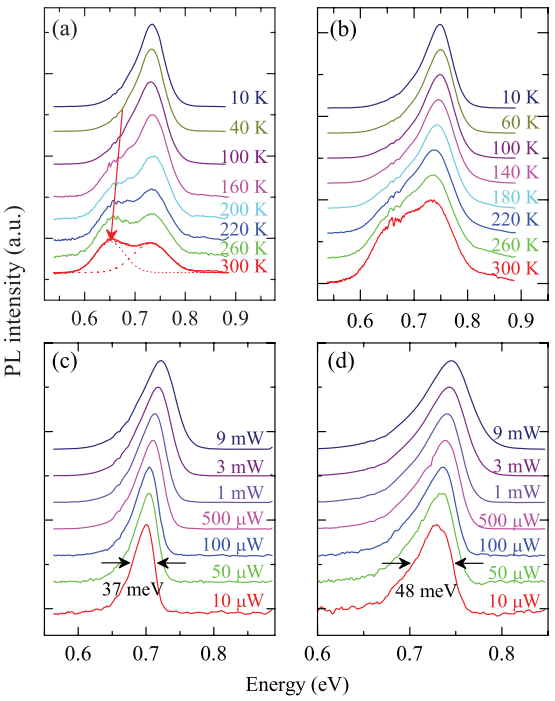

FIG. 3. (Color online) PL spectra of InN:Si nanowires with (a) moderate and (b) heavy Si doping at different temperatures under an excitation power of 9 mW and (c) moderate and (d) heavy Si doping under different optical excitation powers measured at 6 K. The narrowest measured linewidth for each Si-doped sample is labeled by the FWHM value.

The important feature revealed by the temperature-dependent spectra is that $E^L_{\rm PL}$ shows a clear redshift as the temperature increases, while $E^H_{\rm PL}$ is almost temperature invariant, which resembles the profiles measured from n-type degenerate InN nanowires.[8,21,33] Here, we suggest $E^L_{\rm PL}$ and $E^H_{\rm PL}$ can be ascribed to the band-to-band carrier recombination from the low-doped *bulk* region and Mahan exciton emission in the high-doped *near-surface* region. Details will be discussed in Sec. IV.

By further increasing Si doping to $\sim 5 \times 10^{18}$ cm^{-3} [Fig. 3(b)], the PL spectra exhibit similar features. However, the high-energy peak described above ($E^H_{\rm PL}$) shifts to an even larger energy, $E^3_{\rm PL} \sim 0.75$ eV; such a blueshift with increasing doping is consistent with the Burstein-Moss effect. Moreover, the PL spectrum at each temperature is dominated by $E^3_{\rm PL}$, which could suggest that the dominant emission region is $E^3_{\rm PL}$ ($E^H_{\rm PL}$) associated. We will show in Sec. IV that this region is the high-doped near-surface region.

From Figs. 3(a) and 3(b), it can be seen that the temperature-dependent PL spectra of InN:Si nanowires are significantly different from those of undoped InN nanowires [Fig. 2(a)]; such difference can also be seen from the power-dependent PL spectra. Comparing Figs. 2(d), 3(c), and 3(d), it can be seen that as Si dopants are incorporated with increased average doping concentration, the spectral linewidth (Γ, as indicated by arrows) gets much broader under the lowest measured optical excitation powers (5 μW for undoped InN nanowires and 10 μW for InN:Si nanowires). Moreover, Γ has a much reduced excitation power dependence; e.g., Γ is nearly power independent for heavily Si-doped InN nanowires [Fig. 3(d)]. Such nearly power-independent PL characteristics of the presented heavily Si-doped InN nanowires have been commonly reported for n-type degenerate InN nanowires.[8,21,33] We ascribe this to the evolution of the dominant emission region from the low-doped nanowire bulk to the high-doped nanowire near surface.

The presence of two emission regions in InN:Si nanowires, as well as the evolution of the dominant emission region from the bulk to the near surface when Si dopants are incorporated and with increased doping concentration, can be ascribed to the Si dopants being preferentially incorporated in the near-surface region. Such Si-dopant surface segregation will be discussed in detail in Sec. IV.

It is important to mention that, up to this point, the PL peaks of the presented InN:Si nanowires are centered at higher energies compared with those of InN films with similar doping concentrations;[7,9,10] in addition, the PL emission in such InN films also shows considerable dependence on optical excitation power. This could indicate that, due to the large surface-to-volume ratios, the surface of InN nanowires plays an important role in the PL characteristics of n-type InN nanowires. In this sense, the aforementioned two emission regions could only exist in nanowire structure due to the enhanced surface effect.

IV. DISCUSSION

From the previously described results, it is evident that the optical characteristics of InN nanowires change significantly with Si doping. For the undoped InN nanowires, the PL emission can be ascribed to band-to-band recombination and may involve free-exciton emission at low temperatures. The PL characteristics can be further characterized by the strong dependence on temperature and optical excitation power. On the other hand, PL emission spectra of InN:Si nanowires measured at low temperatures resemble those of n-type degenerate InN nanowires, i.e., a peak energy (here ~0.73–0.75 eV) considerably larger than the band gap of InN, as well as the absence of the band-filling effect with increasing optical excitation power.[63] However, with increasing temperature, a new feature, the low-energy peak ($E_{\mathrm{PL}}^{L} \sim 0.65$ eV), emerges in the PL spectra of InN:Si nanowires. In the rest of this paper, we will discuss the origin of this peak as well as the influence of the charge-carrier concentrations and distributions on the optical characteristics of InN nanowires.

In order to address the aforementioned issues, it is critically important to understand the charge-carrier distribution or the Si-dopant distribution in InN nanowires. Although the Si-doping mechanism in InN nanowires remains unclear, the surface segregation of dopant species has been commonly observed in the epitaxially grown III-nitride semiconductors as well as various nanowire structures.[64,65] In order to examine such Si-dopant surface segregation in InN nanowires, the near-surface E_F at the lateral surfaces of undoped and moderately Si-doped InN nanowires is directly investigated by angle-resolved XPS.

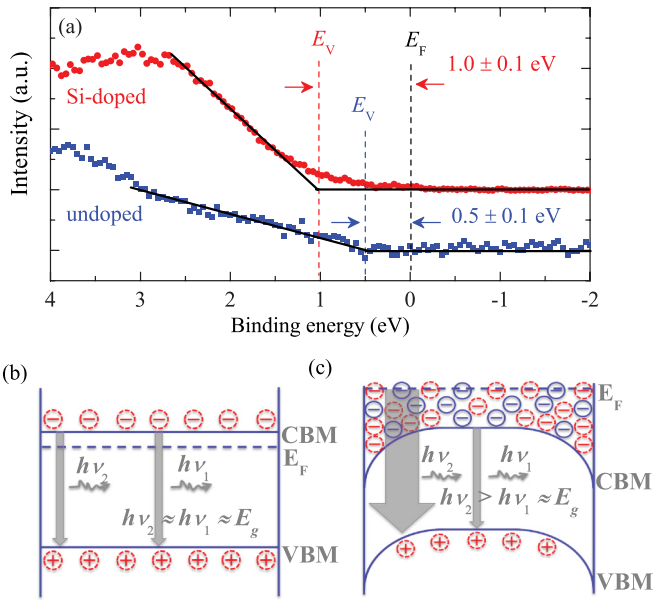

FIG. 4. (Color online) (a) X-ray photoelectron spectroscopy of intrinsic and moderately Si-doped InN nanowires. (b) and (c) show the carrier distributions and recombination processes in intrinsic and InN:Si nanowires, respectively. The blue circles represent residual free charge carriers, and the dotted red circles represent photogenerated charge carriers.

As can be seen from Fig. 4(a), the near-surface E_F for undoped InN nanowires lies well below the CBM [for $E_g(300\ \mathrm{K}) = 0.65$ eV], suggesting the absence of surface electron accumulation and essentially *intrinsic* InN nanowires. In contrast, the near-surface E_F for InN:Si nanowires is measured ~1.0 eV above the valence band maximum (VBM) and hence is pinned to the conduction band with ~0.35 eV above the CBM; this corresponds to a high electron density of $\sim 1 \times 10^{12-13}$ cm^{-2} in the near-surface region,[46] which is significantly larger than the average doping concentration of moderately Si-doped InN nanowires ($\sim 5 \times 10^{17}$ cm^{-3}). These results strongly suggest that the near-surface region of InN:Si nanowires can be characterized by the presence of a large density of electrons and hence is heavily Si doped, while the bulk region of such InN:Si nanowires is therefore characterized by the presence of a low density of electrons and hence is lightly Si doped.[66] We would like to point out that, up to now, such enhanced surface doping is mostly determined by Si dopants other than unintentional n-type defect dopants.[67] A detailed investigation of the surface charge properties of InN nanowires, including tuning the surface band bending and two-dimensional electron gas formation by controlled Si-dopant incorporation and/or wire morphology, is published elsewhere.[46]

Based on the XPS results, the carrier distributions, together with the associated carrier recombination processes, are schematically shown in Figs. 4(b) and 4(c) for intrinsic and Si-doped InN nanowires, respectively. For intrinsic InN nanowires, photogenerated electron-hole pairs may distribute nearly uniformly across the lateral dimension of the nanowires, and the measured PL emission is mainly due to the band-to-band carrier recombination (therefore shrinkage of the band gap and band-filling effect can be clearly observed). For InN:Si nanowires, however, the near-surface region is characterized by the presence of a large density of electrons and hence severe surface band bending.[68] Due to the band-bending-induced lateral electric field, photogenerated electrons preferentially migrate to the near-surface region. In this case, two emission regions, i.e., the bulk region (low doped) and the near-surface region (high doped), could probably exist in InN:Si nanowires; the corresponding energy is marked by $h\nu_1$ and $h\nu_2$, respectively. Moreover, as Si doping increases, the near-surface-region emission could become more important; i.e., the dominant emission region evolves from the low-doped nanowire bulk to the high-doped nanowire near surface. In what follows, we will examine these scenarios and correlate them with the PL characteristics.

Figure 5(a) shows the extracted [by two Gaussian distributions; see the dotted curves in Fig. 3(a) for a sample fitting] temperature-dependent E_{PL}^{L} and E_{PL}^{H} of the moderately Si-doped InN nanowires. E_{PL}^{1} of intrinsic InN nanowires [from Fig. 2(a)] and E_{PL}^{3} of heavily Si-doped InN:Si nanowires [from Fig. 3(b)] are also shown in Fig. 5(a) for comparison. It can be seen that the temperature dependence of E_{PL}^{L} is remarkably similar to that of E_{PL}^{1}; therefore E_{PL}^{L} can be ascribed to carrier recombination in the relatively low-doped region. The temperature dependence of E_{PL}^{H}, on the other hand, is remarkably identical to that of E_{PL}^{3} in heavily Si-doped InN nanowires as well as the commonly observed temperature dependencies of peak energies from the n-type degenerate

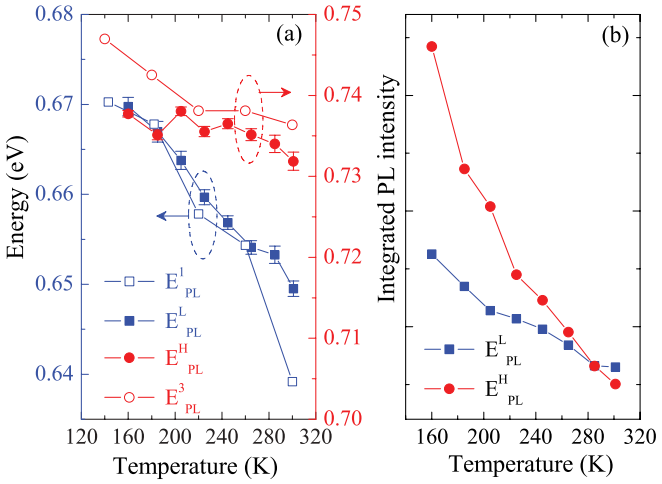

FIG. 5. (Color online) (a) Temperature dependence of peak energies: E_{PL}^{L} from the low-doped bulk region (solid blue squares) and E_{PL}^{H} from the high-doped near-surface region (solid red circles) of moderately Si-doped InN nanowires, E_{PL}^{1} of intrinsic InN nanowires (open blue squares), and E_{PL}^{3} of heavily Si-doped InN nanowires (open red circles). (b) Temperature-dependent integrated PL intensity for the two emission regions of moderately Si-doped InN nanowires.

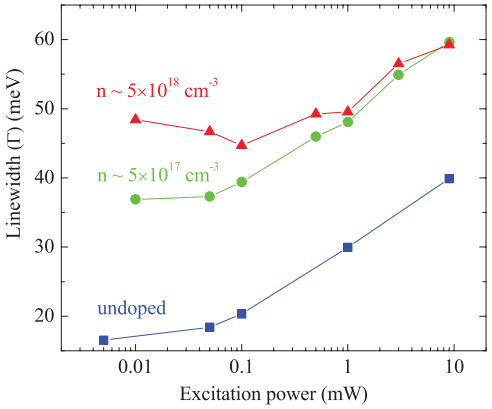

FIG. 6. (Color online) Extracted optical excitation power dependence of spectral linewidths Γ for intrinsic [from Fig. 2(d)] and Si-doped InN nanowires [from Figs. 3(c) and 3(d)] measured at low temperatures.

InN nanowires;[8,21,33] therefore they can be ascribed to carrier recombination in the relatively high-doped region. These results are consistent with InN:Si nanowires being characterized by the presence of relatively low- and high-doped regions, corresponding to the nanowire bulk and nanowire near-surface regions, respectively. This is a natural consequence of an inhomogeneous electron distribution caused by the discussed Si-dopant surface segregation.

More details about PL characteristics in the low-doped (the bulk) and high-doped (the near-surface) regions can be revealed by the extracted temperature-dependent integrated PL intensity corresponding to each region [area under dotted curves in Fig. 3(a)]. As can be seen from Fig. 5(b), with increasing temperature the PL branch from the high-doped region quenches significantly faster than the PL branch from the low-doped region. This fast decay of the PL emission from the high-doped region can also be observed in Fig. 3(a), in which as the temperature increases, the PL emission from the low-doped region gradually dominates the spectra. The fast decay with increasing temperature in the high-doped region can be largely attributed to the significantly enhanced nonradiative recombination rate due to the presence of large surface states and defects. This further confirms that the high-doped region is located in the vicinity of the nanowire surface.[69]

The described scenarios can also be justified by the distinct PL characteristics of intrinsic and Si-doped InN nanowires at low temperatures. As illustrated in Fig. 6, the power-dependent PL spectral linewidths Γ were derived from Figs. 2(d), 3(c), and 3(d) for intrinsic, moderately Si-doped, and heavily Si-doped InN nanowires, respectively. It can be seen that Γ broadens significantly with increasing Si doping (i.e., at fixed optical excitation power), which is directly related to the band bending in the near-surface region and the resulting highly inhomogeneous carrier distributions.

This can be understood within the framework of the Mahan exciton emission. Due to the enhanced surface doping, the energy spacing between E_F and valence band tails varies along the nanowire radial direction. As a result, electrons with a broad energy distribution are involved in the recombination process, resulting in very broad PL emission spectra; such an effect can only be significant in the near-surface region due to the more severe band bending. This broadening with increasing Si doping essentially indicates the near-surface region emission gradually dominates the PL spectra; such an effect can also be observed if one compares the PL spectrum of moderately Si-doped InN nanowires with that of heavily Si-doped InN nanowires measured at 300 K [Figs. 3(a) and 3(b)].

Moreover, it can be seen from the heavily Si-doped InN nanowires that the linewidth Γ shows a small or negligible dependence on optical excitation power, compared to Γ measured from intrinsic InN nanowires. This can also be explained by the fact that at this average Si-doping concentration the photogenerated electron density might be significantly smaller than the accumulated electron density in the near-surface region due to the enhanced surface doping. As a consequence, the PL spectra, in terms of both the peak position and spectral linewidth, are largely determined by the residual electron density in the near-surface region instead of optical excitation power; this is in direct contrast to the case for intrinsic InN nanowires.

In this regard, it is suggested that the broad near-surface region emission predominantly determines the PL characteristics of *n*-type degenerate InN nanowires, thereby leading to a very large and temperature-independent peak energy (considerably larger than the band gap of InN) as well as a very broad and optical excitation power-independent spectral linewidth. However, band-to-band carrier recombination in the relatively low-doped nanowire bulk region may also be *clearly* observed, depending on the residual electron density, as is the case for the moderately Si-doped InN nanowires in this study. Compared to PL characteristics of intrinsic InN nanowires, which can be well explained by the absence or a negligible level of surface electron accumulation at the nonpolar surface, the PL characteristics of InN:Si

nanowires are fundamentally different, which is the natural result of the presence of electron accumulation at the nonpolar surface.

V. CONCLUSIONS

In this work, temperature-dependent PL measurements were performed on both intrinsic and Si-doped InN nanowires. For intrinsic InN nanowires, the PL emission can be attributed to band-to-band carrier recombination and may involve free-exciton emission. The lateral nonpolar surface is characterized by the absence or a negligible level of surface electron accumulation. Detailed analysis of InN:Si nanowires, however, indicates that the near-surface region is much more heavily doped, which results in surface electron accumulation and Fermi-level pinning as well as the associated two emission regions from the low-doped nanowire bulk and the high-doped nanowire near surface. Depending on the doping concentrations and degree of carrier localization, PL emissions in InN:Si nanowires may involve both band-to-band carrier recombination and Mahan exciton emission. These results clearly demonstrate that the optical properties of InN nanowires are closely related to the charge-carrier concentrations and distributions as well as the surface charge properties.

ACKNOWLEDGMENTS

This work was supported by the Natural Sciences and Engineering Research Council of Canada and the Fonds de recherch sur la nature et les technologies. The authors wish to thank Saeed Fathololoumi for his kind assistance with the PL measurements. Part of the work was performed in the Microfabrication Facility at McGill University. Some of the XPS studies were performed at Sandia and were funded by the US DOE Office of Basic Energy Sciences, Division of Materials Science and Engineering. Sandia National Laboratories is a multiprogram laboratory managed and operated by Sandia Corporation, a wholly owned subsidiary of Lockheed Martin Corporation, for the U.S. Department of Energy's National Nuclear Security Administration under Contract No. DE-AC04-94AL85000.

*zetian.mi@mcgill.ca

[1] T. Matsuoka, H. Okamoto, M. Nakao, H. Harima, and E. Kurimoto, Appl. Phys. Lett. **81**, 1246 (2002).
[2] V. Y. Davydov, A. Klochikhin, R. Seisyan, V. Emtsev, S. Ivanov, F. Bechstedt, J. Furthmüller, H. Harima, A. Mudryi, J. Aderhold *et al.*, Phys. Stat. Sol. (b) **229**(3), R1 (2002).
[3] J. Wu, W. Walukiewicz, K. M. Yu, J. W. Ager, E. E. Haller, H. Lu, W. J. Schaff, Y. Saito, and Y. Nanishi, Appl. Phys. Lett. **80**, 3967 (2002).
[4] J. Wu, W. Walukiewicz, W. Shan, K. M. Yu, J. W. Ager III, E. E. Haller, H. Lu, and W. J. Schaff, Phys. Rev. B **66**, 201403 (2002).
[5] J. Wu, W. Walukiewicz, W. Shan, K. M. Yu, J. W. Ager, S. X. Li, E. E. Haller, H. Lu, and W. J. Schaff, J. Appl. Phys. **94**, 4457 (2003).
[6] B. Arnaudov, T. Paskova, P. P. Paskov, B. Magnusson, E. Valcheva, B. Monemar, H. Lu, W. J. Schaff, H. Amano, and I. Akasaki, Phys. Rev. B **69**, 115216 (2004).
[7] S. P. Fu, T. T. Chen, and Y. F. Chen, Semicond. Sci. Technol. **21**, 244 (2006).
[8] T. Stoica, R. J. Meijers, R. Calarco, T. Richter, E. Sutter, and H. Lueth, Nano Lett. **6**, 1541 (2006).
[9] M. Feneberg, J. Däubler, K. Thonke, R. Sauer, P. Schley, and R. Goldhahn, Phys. Rev. B **77**, 245207 (2008).
[10] M. E. Holtz, I. Gherasoiu, V. Kuryatkov, S. A. Nikishin, A. A. Bernussi, and M. W. Holtz, J. Appl. Phys. **105**, 063702 (2009).
[11] J. Segura-Ruiz, N. Garro, A. Cantarero, C. Denker, J. Malindretos, and A. Rizzi, Phys. Rev. B **79**, 115305 (2009).
[12] Y. L. Chang, F. Li, A. Fatehi, and Z. Mi, Nanotechnology **20**, 345203 (2009).
[13] Y. L. Chang, Z. Mi, and F. Li, Adv. Funct. Mater. **20**, 4146 (2010).
[14] M. César, Y. Ke, W. Ji, H. Guo, and Z. Mi, Appl. Phys. Lett. **98**, 202107 (2011).
[15] V. Chin, T. Tansley, and T. Osotchan, J. Appl. Phys. **75**, 7365 (1994).
[16] S. Strite and H. Morkoc, J. Vac. Sci. Technol. B **10**, 1237 (1992).
[17] A. G. Bhuiyan, A. Hashimoto, and A. Yamamoto, J. Appl. Phys. **94**, 2779 (2003).
[18] J. Wu, J. Appl. Phys. **106**, 011101 (2009).
[19] I. Mahboob, T. D. Veal, C. F. McConville, H. Lu, and W. J. Schaff, Phys. Rev. Lett. **92**, 036804 (2004).
[20] I. Mahboob, T. D. Veal, L. F. J. Piper, C. F. McConville, H. Lu, W. J. Schaff, J. Furthmüller, and F. Bechstedt, Phys. Rev. B **69**, 201307(R) (2004).
[21] C. H. Shen, H. Y. Chen, H. W. Lin, S. Gwo, A. A. Klochikhin, and V. Y. Davydov, Appl. Phys. Lett. **88**, 253104 (2006).
[22] E. Calleja, J. Grandal, M. A. Sánchez-García, M. Niebelschütz, V. Cimalla, and O. Ambacher, Appl. Phys. Lett. **90**, 262110 (2007).
[23] C. G. Van de Walle and D. Segev, J. Appl. Phys. **101**, 081704 (2007).
[24] J. Segura-Ruiz, A. Molina-Sánchez, N. Garro, A. García-Cristóbal, A. Cantarero, F. Iikawa, C. Denker, J. Malindretos, and A. Rizzi, Phys. Rev. B **82**, 125319 (2010).
[25] T. Richter, H. Luth, T. Schapers, R. Meijers, K. Jeganathan, S. Estevez Hernandez, R. Calarco, and M. Marso, Nanotechnology **20**, 405206 (2009).
[26] A. Yoshikawa, X. Wang, Y. Ishitani, and A. Uedono, Phys. Status Solidi A **207**, 1011 (2010).
[27] C. G. Van de Walle, J. Lyons, and A. Janotti, Phys. Status Solidi A **207**, 1024 (2010).
[28] T. Stoica and R. Calarco, IEEE J. Sel. Top. Quantum Electron. **17**, 859 (2011).
[29] W. M. Linhart, T. D. Veal, P. D. C. King, G. Koblmüller, C. S. Gallinat, J. S. Speck, and C. F. McConville, Appl. Phys. Lett. **97**, 112103 (2010).
[30] A. Eisenhardt, M. Himmerlich, and S. Krischok, Phys. Status Solidi A **209**, 45 (2012).
[31] M. Moret, S. Ruffenach, O. Briot, and B. Gil, Appl. Phys. Lett. **95**, 031910 (2009).
[32] J. Grandal, M. A. Sánchez-García, E. Calleja, E. Gallardo, J. M. Calleja, E. Luna, A. Trampert, and A. Jahn, Appl. Phys. Lett. **94**, 221908 (2009).

[33]M. A. Sánchez-García, J. Grandal, E. Calleja, S. Lazic, J. M. Calleja, and A. Trampert, Phys. Status Solidi B **243**, 1490 (2006).
[34]F. Werner, F. Limbach, M. Carsten, C. Denker, J. Malindretos, and A. Rizzi, Nano Lett. **9**, 1567 (2009).
[35]S. P. Fu, C. J. Yu, T. T. Chen, G. M. Hsu, M. J. Chen, L. C. Chen, K. H. Chen, and Y. F. Chen, Adv. Mater. **19**, 4524 (2007).
[36]M. Johnson, C. Lee, E. Bourret-Courchesne, S. Konsek, S. Aloni, W. Han, and A. Zettl, Appl. Phys. Lett. **85**, 5670 (2004).
[37]C.-T. Kuo, S.-C. Lin, K.-K. Chang, H.-W. Shiu, L.-Y. Chang, C.-H. Chen, S.-J. Tang, and S. Gwo, Appl. Phys. Lett. **98**, 052101 (2011).
[38]C. Wu, H. Lee, C. Kuo, C. Chen, and S. Gwo, Phys. Rev. Lett. **101**, 106803 (2008).
[39]P. Ebert, S. Schaafhausen, A. Lenz, A. Sabitova, L. Ivanova, M. Dähne, Y. L. Hong, S. Gwo, and H. Eisele, Appl. Phys. Lett. **98**, 062103 (2011).
[40]G. D. Mahan, Phys. Rev. **153**, 882 (1967).
[41]S. P. Fu, Y. F. Chen, and K. Tan, Solid State Commun. **137**, 203 (2006).
[42]A. Mohanta, D. J. Jang, G. T. Lin, Y. T. Lin, and L. W. Tu, J. Appl. Phys. **110**, 023703 (2011).
[43]A. A. Klochikhin, V. Y. Davydov, V. V. Emtsev, A. V. Sakharov, V. A. Kapitonov, B. A. Andreev, H. Lu, and W. J. Schaff, Phys. Rev. B **71**, 195207 (2005).
[44]C. Rauch, F. Reurings, F. Tuomisto, T. D. Veal, C. F. McConville, H. Lu, W. J. Schaff, C. S. Gallinat, G. Koblmüller, J. S. Speck, W. Egger, B. Löwe, L. Ravelli, and S. Sojak, Phys. Status Solidi A **207**, 1083 (2010).
[45]T. Gotschke, E. Schäfer-Nolte, R. Caterino, F. Limbach, T. Stoica, E. Sutter, K. Jeganathan, and R. Calarco, Nanotechnology **22**, 125704 (2011).
[46]S. Zhao, S. Fathololoumi, K. H. Bevan, D. Liu, M. G. Kibria, Q. Li, G. T. Wang, H. Guo, and Z. Mi, Nano Lett., in press, doi: 10.1021/nl300476d.
[47]C. Liang, L. Chen, J. Hwang, K. Chen, Y. Hung, and Y. Chen, Appl. Phys. Lett. **81**, 22 (2002).
[48]J. Zhang, L. Zhang, X. Peng, and X. Wang, J. Mater. Chem. **12**, 802 (2002).
[49]J. Grandal, M. A. Sánchez-García, E. Calleja, E. Luna, and A. Trampert, Appl. Phys. Lett. **91**, 021902 (2007).
[50]J. Grandal and M. Sanchezgarcia, J. Cryst. Growth **278**, 373 (2005).
[51]E. Calleja, J. Ristić, S. Fernández-Garrido, L. Cerutti, M. A. Sánchez-García, J. Grandal, A. Trampert, U. Jahn, G. Sánchez, A. Griol, and B. Sánchez, Phys. Status Solidi B **244**, 2816 (2007).
[52]C. Hsiao, H. Hsu, L. Chen, C. Wu, C. Chen, M. Chen, L. Tu, and K. Chen, Appl. Phys. Lett. **91**, 181912 (2007).
[53]T. B. Hoang, A. F. Moses, H. L. Zhou, D. L. Dheeraj, B. O. Fimland, and H. Weman, Appl. Phys. Lett. **94**, 133105 (2009).
[54]L. V. Titova, T. B. Hoang, H. E. Jackson, L. M. Smith, J. M. Yarrison-Rice, Y. Kim, H. J. Joyce, H. H. Tan, and C. Jagadish, Appl. Phys. Lett. **89**, 173126 (2006).
[55]A. Mishra, L. V. Titova, T. B. Hoang, H. E. Jackson, L. M. Smith, J. M. Yarrison-Rice, Y. Kim, H. J. Joyce, Q. Gao, H. H. Tan, and C. Jagadish, Appl. Phys. Lett. **91**, 263104 (2007).
[56]A. Chiari, M. Colocci, F. Fermi, Y. Li, R. Querzoli, A. Vinattieri, and W. Zhuang, Phys. Status Solidi B **147**, 421 (1988).
[57]S. Breuer, C. Pfuller, T. Flissikowski, O. Brandt, H. T. Grahn, L. Geelhaar, and H. Riechert, Nano Lett. **11**, 1276 (2011).
[58]F. Bernardini, V. Fiorentini, and D. Vanderbilt, Phys. Rev. Lett. **79**, 3958 (1997).
[59]S. P. Fu and Y. Chen, Appl. Phys. Lett. **85**, 1523 (2004).
[60]T. Schmidt, K. Lischka, and W. Zulehner, Phys. Rev. B **45**, 8989 (1992).
[61]However, the PL peak energy maintains more or less the same value, ∼0.674 eV. For details, see Ref. 46.
[62]For moderately Si-doped InN nanowires, secondary ion mass spectroscopy indicates the Si-doped concentration is $\sim 5 \times 10^{17}$ cm^{-3}. For a Si cell temperature difference of ∼100 °C, in general, the Si-doping concentration will vary by another factor of ∼10.
[63]As discussed in Sec. IV, due to the enhanced n-type characteristics, similar approaches (as those for undoped InN nanowires) did not find evidence of excitons.
[64]P. Xie, Y. Hu, Y. Fang, J. Huang, and C. Lieber, Proc. Natl. Acad. Sci. **106**, 15254 (2009).
[65]D. Perea, E. Hemesath, E. Schwalbach, J. Lensch-Falk, P. Voorhees, and L. Lauhon, Nat. Nanotechnol. **4**, 315 (2009).
[66]The *ab initio* calculations (see Ref. 46) indicate the dopant (either Si donors or defect donors) formation energy is much lower in the near-surface region (particularly within the first ∼0.5 nm) than in the bulk region; this is the reason for the dopant surface segregation, and as a consequence, E_F is pinned to the conduction band in the near-surface region.
[67]Another separate study (see Ref. 46) suggests that if other n-type defect donors exist, E_F at the near-surface region will be pinned to a higher energy.
[68]See Ref. 46; the flat band situation cannot explain the presence of high electron density in the near-surface region and low electron density in the bulk region.
[69]The low-energy peak E_{PL}^{L} is not observable at low temperatures. This is because (1) E_{PL}^{L} shifts to higher energy at low temperatures and it merges with E_{PL}^{H} [see Fig. 3(a)], and (2) the intensity of E_{PL}^{H} increases much faster than that of E_{PL}^{L} with decreasing temperature such that E_{PL}^{H} overshadows E_{PL}^{L} at low temperatures [see Fig. 5(a)]. The reason for this can be ascribed to the evolution of the emission region to the near-surface as discussed in the main text, as well as the reduced nonradiative recombination rate in the near-surface region at low temperatures.